Rheologica Acta (2023) 62:269–283
https://doi.org/10.1007/s00397-023-01393-0

ORIGINAL CONTRIBUTION

Modeling elongational viscosity and brittle fracture of 10 polystyrene Pom-Poms by the hierarchical molecular stress function model

Valerian Hirschberg[1] · Max G. Schußmann[1] · Marie-Christin Röpert[1] · Manfred Wilhelm[1] · Manfred H. Wagner[2]

Received: 15 December 2022 / Revised: 14 February 2023 / Accepted: 19 March 2023 / Published online: 5 April 2023

Abstract

A Pom-Pom polymer with q_a side chains of molecular weight $M_{w,a}$ at both ends of a backbone chain of molecular weight $M_{w,b}$ is the simplest branched polymer topology. Ten nearly monodisperse polystyrene Pom-Pom systems synthesized via an optimized anionic polymerization and a grafting-onto method with $M_{w,b}$ of 100 to 400 kg/mol, $M_{w,a}$ of 9 to 50 kg/mol, and q_a between 9 and 22 are considered. We analyze the elongational rheology of the Pom-Poms by use of the hierarchical multi-mode molecular stress function (HMMSF) model, which has been shown to predict the elongational viscosity of linear and long-chain branched (LCB) polymer melts based exclusively on the linear-viscoelastic characterization and a single material parameter, the so-called dilution modulus G_D. For the Pom-Poms considered here, we show that G_D can be identified with the plateau modulus $G_N^0 = G_D$, and the modeling of the elongational viscosity of the Pom-Poms does therefore not require any fitting parameter but is fully determined by the linear-viscoelastic characterization of the melts. Due to the high strain hardening of the Pom-Poms, brittle fracture is observed at higher strains and strain rates, which is well described by the entropic fracture criterion.

Keywords Polystyrene · Long-chain branching · Elongational viscosity · Strain hardening · HMMSF model · Entropic fracture criterion

Introduction

With the demand for a more sustainable use of polymeric materials, it is of utmost importance to ensure enhanced processing properties and recyclability. For processing, the optimization of thinning in shear and hardening in elongational flow of polymer melts are both especially favorable. Topology is a key parameter to control the melt rheological properties of a polymer; thus, its processing allows to tune melt properties of recycled polymer melts via the addition of small amounts of specially designed topologies. Consequently, topology allows tuning rheological properties beyond the ones for linear polymers predicted with reptation theory, e.g., an increase in zero-shear viscosity scaling with the average weight molecular weight by an exponent of 3, or rather 3.4, so $\eta_0 \sim M_w^{3.4}$ (Larson 1999). Common but still defined branched topologies of interest are star, comb, H-shaped, and the so-called Pom-Pom topology. In the latter, two stars are covalently connected by a linear chain. Due to the high effort to synthesize the Pom-Pom topology in the gram dimension, the focus in literature is mainly on linear (Ianniruberto et al. 2020; Matsumiya et al. 2018; Nielsen et al. 2006a), star (Frischknecht et al. 2002; Graessley and Roovers 1979), and comb structures (Abbasi et al. 2017; Kapnistos et al. 2005; Lentzakis et al. 2013; Roovers and Graessley 1981), and only a few studies on H-shaped (Ianniello and Costanzo 2022; Lentzakis et al. 2019) and Pom-Pom polymers (Houli et al. 2002; Nielsen et al. 2006b; van Ruymbeke et al. 2007) have been reported.

Following the idea of the tube model, strain hardening is created on the molecular level by chain stretching (Larson 1999; McLeish and Larson 1998). In elongational flow, linear

Dedicated to the memory of Prof. Thomas Charles Buckland McLeish FRS.

✉ Valerian Hirschberg
valerian.hirschberg@kit.edu

✉ Manfred H. Wagner
manfred.wagner@tu-berlin.de

[1] Institute of Chemical Technology and Polymer Chemistry (ITCP), Karlsruhe Institute of Technology (KIT), Engesserstraße 18, 76131 Karlsruhe, Germany

[2] Polymer Engineering/Polymer Physics, Berlin Institute of Technology (TU Berlin), Ernst-Reuter-Platz 1, 10587 Berlin, Germany

low-disperse polymers show rather weak strain hardening at strain rates above the inverse of the Rouse relaxation time, τ_R, and no strain hardening can be observed at strain rates below the inverse of τ_R (Matsumiya and Watanabe 2021). However, higher processing temperatures that reduce the Rouse relaxation time τ_R are very beneficial for processing as they reduce the shear viscosity, so strain hardening at high temperatures is extremely desirable. It is commonly known that strain hardening can be induced by long-chain branching (LCB) (Huang 2022; Larson 1999; Stadler et al. 2009). The resistance of the branch points to be pulled into the backbone tube increases the stress in the backbone leading to the stretch of the segments between two branching points (Huang). To induce strain hardening via topology in elongational flow, at least two branching points in the polymer molecule are needed. Consequently, the H-shaped and the Pom-Pom topology are the simplest topologies that provide exactly two branching points with a sidechain number $q \geq 2$ at each end of the backbone (McLeish et al. 1999). In general, the Pom-Pom topology combines two properties that are very favorable for processing: (i) thinning under shear deformation and (ii) strain hardening in elongational flow. Low-density polyethylene (LDPE) is a commonly used strain hardening polymer, with a strain hardening factor (SHF) typical around SHF = 10. However, LDPE has an ill-defined comb-shaped and branch-on-branch topology (Wagner et al. 2004). SHF above 10 have been observed for branched polystyrene (PS) model structures with at least two branching points, such as comb (Abbasi et al. 2017, 2019; Faust et al. 2022; Kempf et al. 2013; Lentzakis et al. 2013), branch-on-branch (Faust et al. 2022), Pom-Pom (Röpert et al. 2022a), barbwire (Röpert et al. 2022b), or Cayley-tree (van Ruymbeke et al. 2010) topologies. Consequently, the molecular design of branched polymers and the prediction of the resulting shear and elongational properties are of considerable interest.

Many constitutive models have been proposed to understand and predict the shear and extensional rheology of polymers, such as the Doi-Edwards (DE) model (Doi and Edwards 1978, 1979). However, the original DE model does not predict strain hardening in elongational flow, since it assumed a constant tube diameter during stretching. Later models like the molecular stress function (MSF) model (Wagner et al. 2001) and models based on it, such as the hierarchical multimode MSF (HMMSF) model (Narimissa and Wagner 2016c), consider changes in the tube diameter. The target of the HMMSF model is to fully predict strain hardening in elongational flow based on the linear rheological response in small amplitude oscillatory shear (SAOS) flow, which reflects the impact of the topology of a polymer on its rheology. Besides elongational flow, current research introduced the concept of brittle fracture at higher strain rates in elongational flow (Huang et al. 2016; Huang and Hassager 2017; Wagner et al. 2018, 2022), i.e., the rupture of the polymer sample with a clear fracture surface instead of steady-state elongational flow. Brittle fracture occurs according to the entropic fracture criterion (Wagner et al. 2018) when the strain energy of a stretched entanglement segment exceeds its bond-dissociation energy of a single carbon–carbon bond.

To fully turn around the molecular design arrow of polymers, not only the development of constitutive models, but also their validation with well-defined model systems is of utmost importance. Due to the so far limited availability of Pom-Pom model systems, no broad systematic study of the impact of topological parameters on the elongational properties and their modeling with constitutive models exists. For example, Nielsen and coworkers investigated the elongational rheology of one PS Pom-Pom model systems with about 2–3 entangled arms (Nielsen et al. 2006b), and van Ruymbeke and coworkers studied the linear viscoelasticity of 6 systems with about 5 unentangled arms of $M_{w,a} = 5$ kg/mol and increasing backbone molecular weight (van Ruymbeke et al. 2007). Since shear thinning and strain hardening originates from the difference in relaxation times between the backbone and the arms, the number of arms (i.e., the backbone volume fraction) is expected to be an important parameter.

We synthesized a series of 10 PS Pom-Pom model systems using a straight-forward synthetic route that offers full control over the topological parameters of a Pom-Pom molecule, including molecular weight of the backbone $M_{w,b}$, the molecular weight of the arm $M_{w,a}$, and the number of the arms q_a. We present and analyze here the linear and nonlinear rheological data of ten Pom-Pom model systems with the following systematically varied molecular properties: the molecular weight of the backbone $M_{w,b}$ spans from 100 to 400 kg/mol, the molecular weight of the arms $M_{w,a}$ varies from 9 to 50 kg/mol, and the number of arms q_a varies between 9 and 22 arms per star and backbone end. We demonstrate that the HMMSF model can well predict the elongational behavior of the ten Pom-Pom model systems by only using the linear-viscoelastic material response in SAOS as input parameter and without the use of any further model parameter. Furthermore, the brittle fracture observed at higher Hencky strains and higher strain rates is well predicted by the entropic fracture criterion.

Materials and experimental methods

Polystyrene Pom-Poms were synthesized in a three-step synthesis by living anionic polymerization. The Pom-Pom backbone was synthesized by a stepwise addition of isoprene and styrene to obtain a polyisoprene-*b*-polystyrene-*b*-polyisoprene (ISI) triblock copolymer followed by subsequent epoxidation of the polyisoprene (PI) blocks (Röpert et al. 2022a). Living PS anions were then grafted onto the backbone, resulting on a

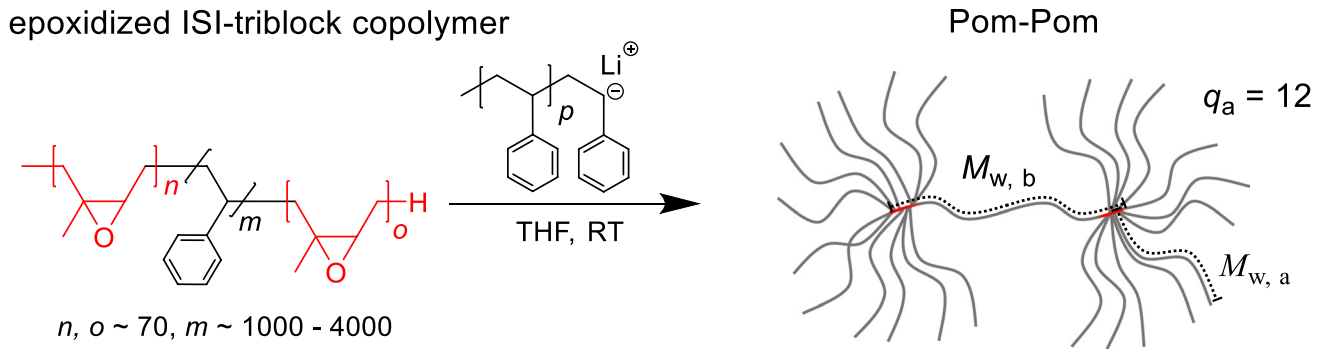

Fig. 1 Synthesis of PS Pom-Poms by grafting of living PS anions onto the epoxidized PI blocks of an ISI triblock copolymer

Table 1 Molecular parameters of the 10 synthesized PS Pom-Poms. $M_{w,b}$ is the weight average molecular weight of the backbone, $M_{w,a}$ the weight average molecular weight of the arms, q_a the number of arms per star/Pom, and $Đ_b$, $Đ_a$, and $Đ_t$ the polydispersity of backbone, arm, and the total molecule

Sample	$M_{w,b}$ [kg/mol]	$Đ_b$	$M_{w,a}$ [kg/mol]	$Đ_a$	$M_{w,total}$ [kg/mol]	q_a	$Đ_t$
POM-POM $M_{w,b}$ – 2xq_a – $M_{w,a}$							
100 k-2×11-9 k	100	1.05	9	1.02	298	2×11	1.13
100 k-2×12-24 k	100	1.05	24	1.05	600	2×12	1.18
100 k-2×12-40 k	100	1.05	40	1.08	1060	2×12	1.16
100 k-2×14-50 k	100	1.05	50	1.20	1500	2×14	1.27
100 k-2×22-25 k	100	1.05	25	1.15	1200	2×22	1.15
220 k-2×9-25 k	220	1.06	25	1.08	670	2×9	1.08
220 k-2×10-40 k	220	1.06	40	1.10	1020	2×10	1.09
280 k-2×22-22 k	280	1.04	22	1.07	1248	2×22	1.15
400 k-2×9-23 k	400	1.10	23	1.14	814	2×9	1.15
400 k-2×13-40 k	400	1.10	40	1.15	1360	2×13	1.15

Pom-Pom-shaped polymer with precise control over backbone length, arm length, and number (Fig. 1). It is important to emphasize that especially the stepwise synthesis of backbone and arms and the subsequent grafting onto give full control over their molecular properties and prevent contaminations with, e.g., stars and limit residual linear chains. More details can be found in literature (Moingeon et al. 2012; Yuan and Gauthier 2005) and earlier works (Röpert et al. 2022a).

Ten different Pom-Pom model systems with low polydispersity were synthesized, by systematically varying $M_{w,b}$, $M_{w,a}$ and q_a. The molecular characteristics can be found in Table 1, with $M_{w,b}$ in the range of 100 to 400 kg/mol, $M_{w,a}$ from 9 to 50 kg/mol, and q_a from 9 to 22 per star. The samples are labeled $M_{w,b}$–2x q_a-$M_{w,a}$.

Oscillatory shear and uniaxial extensional measurements were performed on an ARES-G2 rheometer (TA Instruments, Newcastle, USA). Oscillatory shear measurements were conducted using a 13-mm plate-plate geometry within a frequency range of $\omega = 0.01 - 100$ rad/s and temperatures between $T = 125$–240 °C. Uniaxial extensional measurements were conducted using an extensional viscosity fixture (EVF) with Hencky strain rates of $\dot{\varepsilon} = 10$–0.01 s^{-1} and temperatures between $T = 140$–180 °C up to a maximum Hencky strain of $\varepsilon = 4$. Samples were hot-pressed at 180 °C for 10 min under vacuum. For details see Röpert et al. (2022a, b).

Linear-viscoelastic characterization

Mastercurves of storage and loss modulus, G' and G'', were obtained for all ten Pom-Poms by time–temperature superposition (TTS) at the reference temperature T_r of 160 °C and are shown in Figs. 2, 3, and 4 and in the Support Information (SI), Figs. SI.1–10. The mastercurves were fitted by parsimonious relaxation spectra for characterization of the linear-viscoelastic relaxation modulus $G(t)$,

$$G(t) = \sum_i G_i(t) = \sum_i g_i \exp\left(t/\pi_i\right) \tag{1}$$

The partial moduli g_i and relaxation times τ_i as determined by the IRIS software (Poh et al. 2022; Winter and Mours 2006) are in excellent agreement with the linear-viscoelastic data of G' and G'' and are also summarized in the SI (Tables SI.1–3).

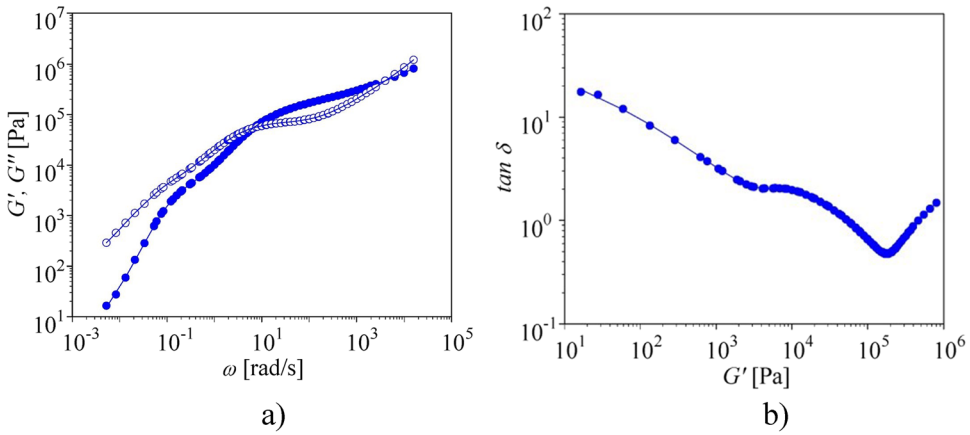

Fig. 2 Experimental data (symbols) of **a** storage (G′) and loss (G″) modulus as a function of the angular frequency as well as **b** loss tanδ vs. G' for Pom-Pom 100 k-2×12-40 k. Lines are fit by parsimonious relaxation spectrum

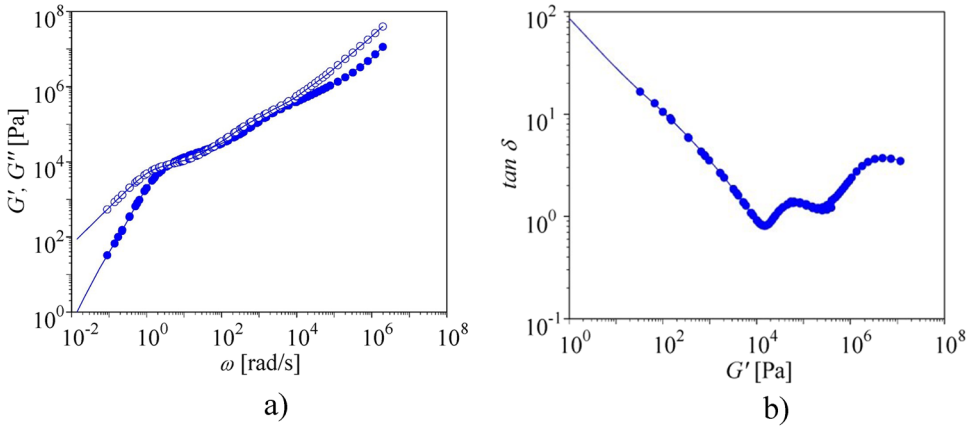

Fig. 3 Experimental data (symbols) of **a** storage (G′) and loss (G″) modulus as a function of the angular frequency as well as **b** loss tanδ vs. G′ for Pom-Pom 100 k-2×11-9 k. Lines are fit by parsimonious relaxation spectrum

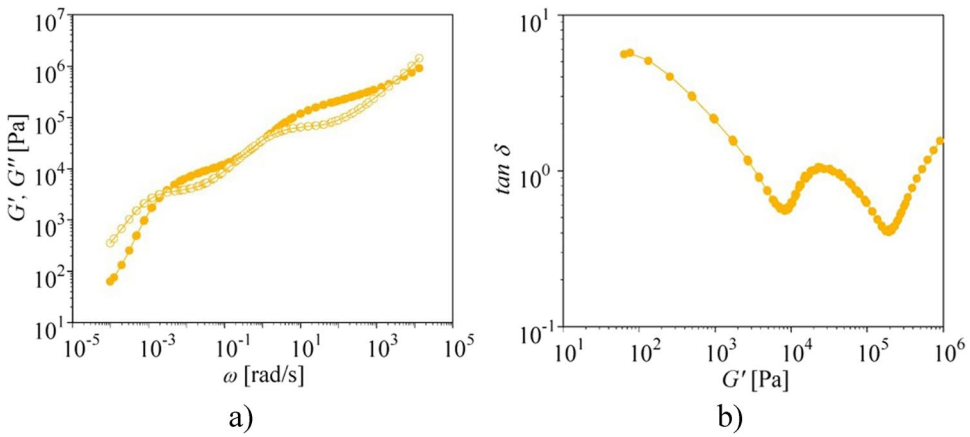

Fig. 4 Experimental data (symbols) of **a** storage (G′) and loss (G″) modulus as a function of the angular frequency as well as **b** loss tanδ as a function of G′ for Pom-Pom 220 k-2×10-40 k. Lines are fit by parsimonious relaxation spectrum

The mass fraction φ_{BB} of the backbone is given by,

$$\varphi_{BB} = \frac{M_{w,b}}{2q_a M_{w,a} + M_{w,b}} \tag{2}$$

For homopolymers, the mass fraction is to very good approximation equal to the volume fraction. Due to the high number of arms ($9 \leq q \leq 22$), four of the five Pom-Poms with backbone molecular weight of $M_{w,b} = 100 kg/mol$ have volume fractions of $\varphi_{BB} \leq 0.15$ and show only one low-frequency cross-over of G' and G''. After dynamic relaxation of the arms, the backbones are unentangled and relax by constraint Rouse relaxation. As an example, Fig. 2 shows the mastercurves of G' and G'' for the system 100 k-2×12-40 k, as well as the corresponding plot of the loss tangent δ as a function of G'. We identify the plateau modulus G_N^0 with the value of the storage modulus G' at the high frequency

Table 2 Pom-Pom backbone molecular weight $M_{w,b}$, backbone mass fraction φ_{BB}, plateau modulus G_N^0, solution modulus $G_{N,s}^0$, zero-shear viscosityη_0, and whether the backbone is self-entangled or not

Sample	$M_{W,BB}$ [kg/mol]	φ_{BB} [-]	G_N^0 [kPa]	$G_{N,s}^0$ [kPa]	η_0 [Pa s]	Self-entangled backbone
100 k-2×11-9 k	100	0.34	260	15	$6.3{\cdot}10^3$	✓
100 k-2×12-24 k	100	0.15	230	5.3	$2.6{\cdot}10^4$	-
100 k-2×12-40 k	100	0.09	190	4.4	$5.6{\cdot}10^4$	-
100 k-2×14-50 k	100	0.07	110	1.1	$2.1{\cdot}10^5$	-
100 k-2×22-25 k	100	0.09	250	4.2	$1.7{\cdot}10^4$	-
220 k-2×9-25 k	220	0.33	230	15	$1.5{\cdot}10^6$	✓
220 k-2×10-40 k	220	0.22	190	8.7	$4.8{\cdot}10^6$	✓
280 k-2×22-22 k	280	0.22	240	14	$8.3{\cdot}10^5$	✓
400 k-2×9-23 k	400	0.49	150	44	$1.9{\cdot}10^7$	✓
400 k-2×13-40 k	400	0.28	180	18	$3.5{\cdot}10^7$	✓

G' minimum of the loss tangent δ. The dynamically diluted backbone chains create a shallow minimum at a lower value of G', which we designate as the "solution modulus"$G_{N,s}^0$. The values of G_N^0 and $G_{N,s}^0$ as well as the zero-shear viscosity η_0 of all ten Pom-Poms are summarized in Table 2.

In Fig. 3, the Pom-Pom 100 k-2×11-9 k with short unentangled arms and a volume fraction of $\varphi_{BB} = 0.34$ shows 2 well-defined minima of tanδ, with the larger G' value representing the plateau modulus G_N^0, while the lower G' value represents the plateau modulus $G_{N,s}^0$ of the dynamically diluted but still entangled backbone chains.

The Pom-Poms with longer backbone chains have higher volume fractions of the backbone φ_{BB} and show two distinct minima of tanδ, representing the plateau modulus G_N^0 of the Pom-Pom molecule and the plateau modulus $G_{N,s}^0$ of the dynamically diluted backbone chains. As an example, Fig. 4 presents the mastercurves of G' and G'' for the system 220 k-2×10-40 k with $\varphi_{BB} = 0.22$, as well as the corresponding plot of tanδ as a function of G'.

The plateau moduli G_N^0 summarized in Table 2 are on the order of $G_N^0 \approx 200kPa$ as expected for PS. The low plateau modulus of Pom-Pom sample 100 k-2×14-50 k is most probably caused by unreacted side chains and remaining traces of solvent and coincides with a larger polydispersity (see Table 1).

For PS comb polymers, Abbasi et al. (2017) have experimentally demonstrated that the dynamically diluted modulus $G_{N,s}^0$ is related to the plateau modulus G_N^0 of linear PS by the relation:

$$G_{N,s}^0 = G_N^0 \varphi_{BB}^2 \tag{3}$$

Figure 5 shows the normalized solution modulus $G_{N,s}^0$ of the PS comb polymers investigated by Abbasi et al. (2017) and of the Pom-Poms investigated here as a function of the backbone fraction ϕ_{BB}. The ratio $G_{N,s}^0/G_{N,s}^0$ is independent of permanent dilution by traces of remaining solvent as was shown by prolonged drying of sample 100 k-2×14-50 k. For

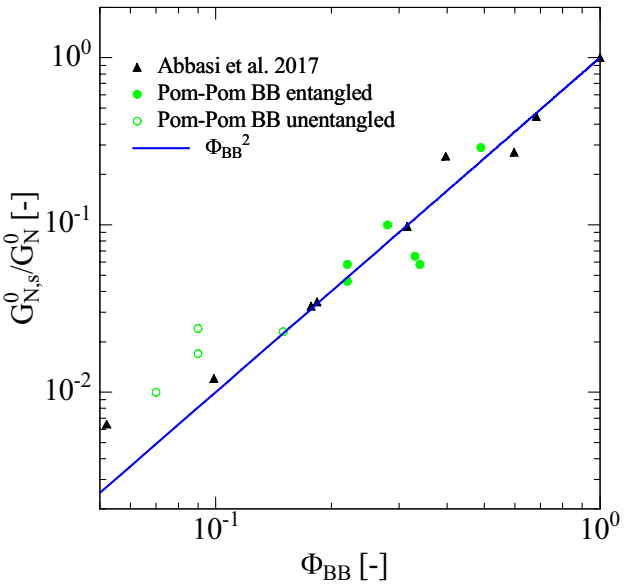

Fig. 5 Normalized solution modulus $G_{N,s}^0$ of PS comb polymers (Abbasi et al. 2017) and Pom-Poms. The blue line indicates φ_{BB}^2 according to Eq. (3)

$\varphi_{BB} \geq 0.1$, all systems follow approximately the Relation (3), while for Pom-Poms with lower values of φ_{BB}, when the backbone is not self-entangled after dynamic dilution, the solution modulus $G_{N,s}^0$ as determined from the shallow minimum of tanδ (see, e.g., Fig. 2) is higher than expected.

Hierarchical molecular stress function (HMMSF) model

The hierarchical multi-mode molecular stress function (HMMSF) model was developed by Narimissa and Wagner for the prediction of uniaxial (Narimissa et al. 2015), multiaxial (Narimissa et al. 2016), and shear (Narimissa and Wagner 2016b) rheological behaviors of polydisperse

long-chain branched (LCB) polymer melts as well as polydisperse linear melts (Narimissa and Wagner 2016a, 2016c). It is based on the linear-viscoelastic relaxation modulus and the concepts of hierarchical relaxation, dynamic dilution, and interchain tube pressure. A summary of the development of the HMMSF model was presented in Narimissa and Wagner (2019a), and a comparison between this model and other prominent tube models for polydisperse linear and long-chain branched polymer melts was given in Narimissa and Wagner (2019b). We shortly summarize the basic equations of the HMMSF model:

The extra stress tensor of the HMMSF is given by,

$$\sigma(t) = \sum_i \int_{-\infty}^{+\infty} \frac{\partial G_i\left(t-t'\right)}{\partial t'} f_i^2(t,t')\mathbf{S}_{DE}^{IA}(t,t')dt' \tag{4}$$

The extra stress is a sum over all stress contributions from discrete Maxwell modes making up the relaxation modulus as defined by Eq. (1), and S_{DE}^{IA} is the Doi and Edwards orientation tensor with the independent alignment (IA) assumption (Doi and Edwards 1978), which is equal to 5 times the second-order orientation tensor **S**. The molecular stress functions $f_i = f_i(t,t')$ are functions of observation time t and the time of creation of tube segments by reptation at time t' and are obtained by integration of the evolution equations,

$$\frac{\partial f_i}{\partial t} = f_i(\mathbf{K}:\mathbf{S}) - \frac{1}{\alpha}\left(\frac{1}{\tau_i} + \beta CR\right)\left[(f_i-1)\left(1-\frac{2}{3}w_i^2\right) + \frac{2}{9}f_i^2\left(f_i^3-1\right)w_i^2\right] \tag{5}$$

K is the velocity gradient tensor and α a topological parameter which depends on the architecture of the chain,

$$\begin{aligned} a &= 1 \quad \text{for LCB melts} \\ a &= 1/3 \ \text{for Linear melts} \end{aligned} \tag{6}$$

CR is a dissipative constraint release term which has non-zero values only in shear flow and is zero in extensional flows (Narimissa and Wagner 2016b).

The mass fractions w_i of chain segments in the evolution Eq. (5) take into account hierarchical dynamic relaxation and are determined by,

$$\begin{aligned} w_i^2 &= \frac{G(t=\tau_i)}{G_D} = \frac{1}{G_D}\sum_{j=1}^{n} g_j \ \exp(-\tau_i/\tau_j) \ \text{ for } \tau_i > \tau_D \\ w_i^2 &= 1 \qquad\qquad\qquad\qquad\qquad\quad \text{for } \tau_i \le \tau_D \end{aligned}, \tag{7}$$

The mass fraction w_i of dynamically diluted segments with relaxation time τ_i longer than the dilution relaxation time τ_D is smaller than 1, while the mass fraction of permanently diluted segments with $\tau_i \le \tau_D$ is set equal to 1. G_D is called the "dilution modulus." The HMMSF model requires a single fitting parameter for extensional flows (i.e., G_D). However, for the model PS Pom-Poms considered here, we can identify G_D with the plateau modulus G_N^0 (Table 2) determined by linear viscoelasticity, because for the low-disperse Pom-Pom melts with many side arms, dynamic dilution is expected to start by hierarchical relaxation of the arms followed by relaxation of the backbone chains. In this way, also the permanent dilution caused by possibly remaining traces of solvent is taken into account. It is important to note that the modeling of the elongational viscosity of the Pom-Poms considered here does not require a fitting parameter, but is fully determined by the linear-viscoelastic characterization of the melts.

At Hencky strains greater than $\varepsilon \approx 4$ and higher strain rates, the elongational stress growth coefficient of long-chain branched (LCB) polymer melts such as low-density polyethylene (LDPE) shows an overshoot due to branch point withdrawal before reaching a steady-state elongational viscosity. This can be accounted for by the extended hierarchical multi-mode molecular stress function (EHMMSF) model (Wagner et al. 2022), which introduces a stretch parameter characterizing the specific Hencky strain at the maximum of the tensile stress. Good agreement was found between experimental data of five LDPE melts with widely different molecular weights, polydispersities and densities, and predictions of the EHMMSF model. We do not consider the EHMMSF model here, as the elongational data of the Pom-Poms investigated are limited to $\varepsilon \le 4$, and due to their high elasticity, sample failure at even lower Hencky strains is observed in elongational flow due to brittle fracture.

Brittle fracture is modeled by the entropic fracture criterion of Wagner et al. (2022): fracture occurs as soon as the entanglement segments correspond to at least one relaxation mode fracture, i.e., when the strain energy of these segments $W = 3kTf_i^2 w_i$ reaches the critical value U, which is the bond-dissociation energy of a single carbon-carbon bond in hydrocarbons. The ratio of the bond-dissociation energy U to the thermal energy $3kT$ is $U/3kT \approx 32$ at $T = 160\ °C$. When the strain energy of the entanglement segment corresponding to mode i reaches the critical value $W_c = U$, the total strain energy of the chain segment is concentrated on one C-C bond by thermal fluctuations, and the bond ruptures. This leads to crack initiation, and within a few milliseconds (Huang et al. 2016; Huang and Hassager 2017), brittle fracture of the sample occurs. From the critical fracture energy $W_c = 3kTf_{i,c}^2 w_i = U$, the square of the critical stretch at fracture, $f_{i,c}^2$, is given by

$$f_{i,c}^2 = \frac{U}{3kT}\frac{1}{w_i} = \frac{32}{w_i} \tag{8}$$

For all Pom-Pom melts investigated here, fracture is first triggered by the mode with the longest relaxation time, followed with increasing strain rates by fracture of polymer chains corresponding to shorter and shorter relaxation modes. At very high elongation rates $\dot{\varepsilon}$, a maximal fracture stress $\sigma_E^{Fractrue}$ is expected with

$$\lim(\sigma_E^{Fractrue})_{\dot{\varepsilon}\to\infty} = 5\sum_i g_i f_i^2 \cong 5\frac{U}{3kT}\sum_i g_i = 160G_N^0 \tag{9}$$

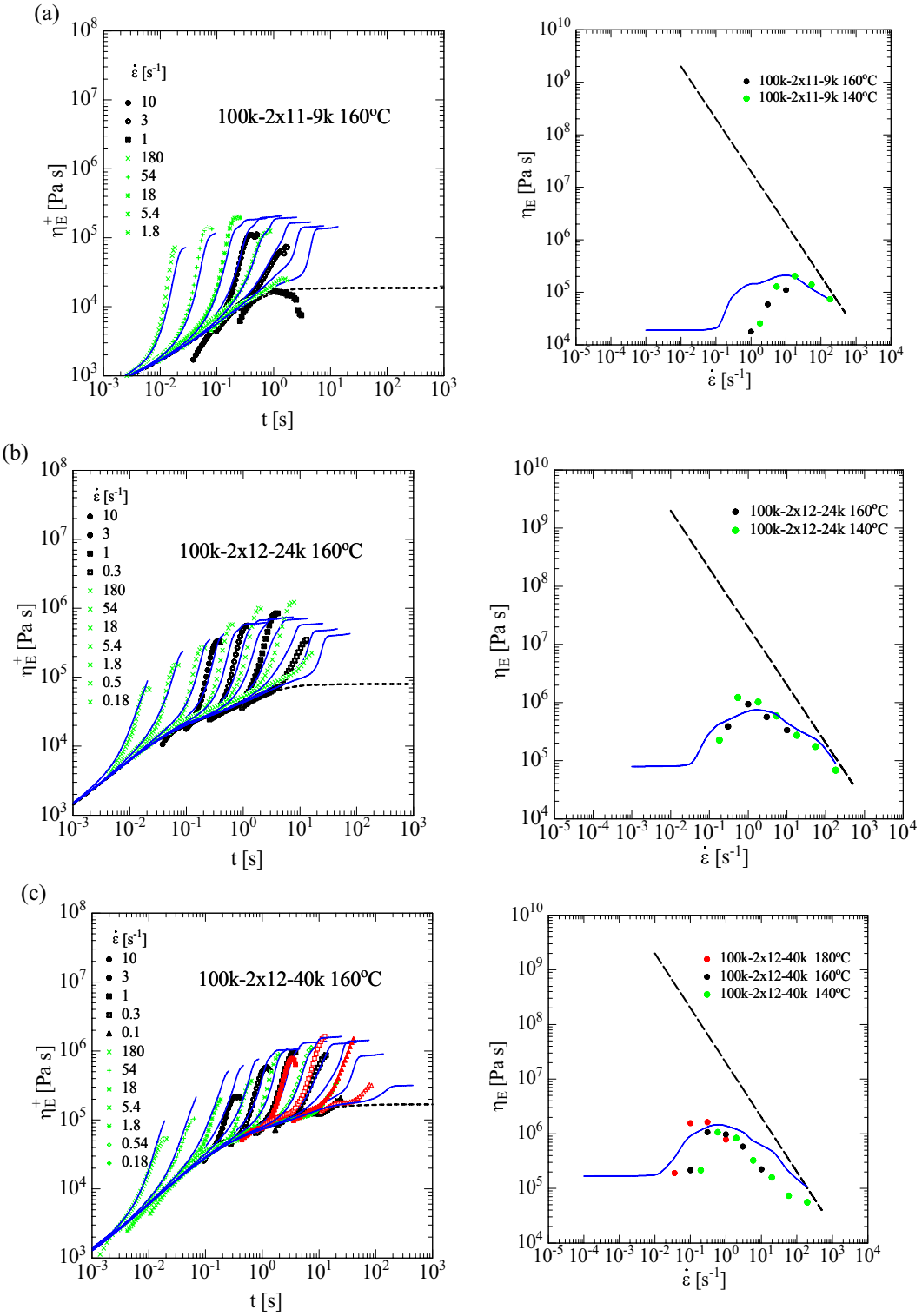

Fig. 6 Elongational stress growth coefficient $\eta_E^+(t)$ and maximal elongational viscosity $\eta_E(\dot{\epsilon})$ in **a** to **j** for the 10 Pom-Pom model systems. Data (symbols) measured at 140 °C (green), 160 °C (black), and 180 °C (red) are shifted to reference temperature of 160 °C. Lines are predictions of the HMMSF model. Dotted lines indicate elongational start-up viscosities $\eta_E(t)$, and broken straight lines with slope of −1 represent a limiting fracture stress of $\sigma_E^{Fracture} = 2.0 \times 10^7$Pa

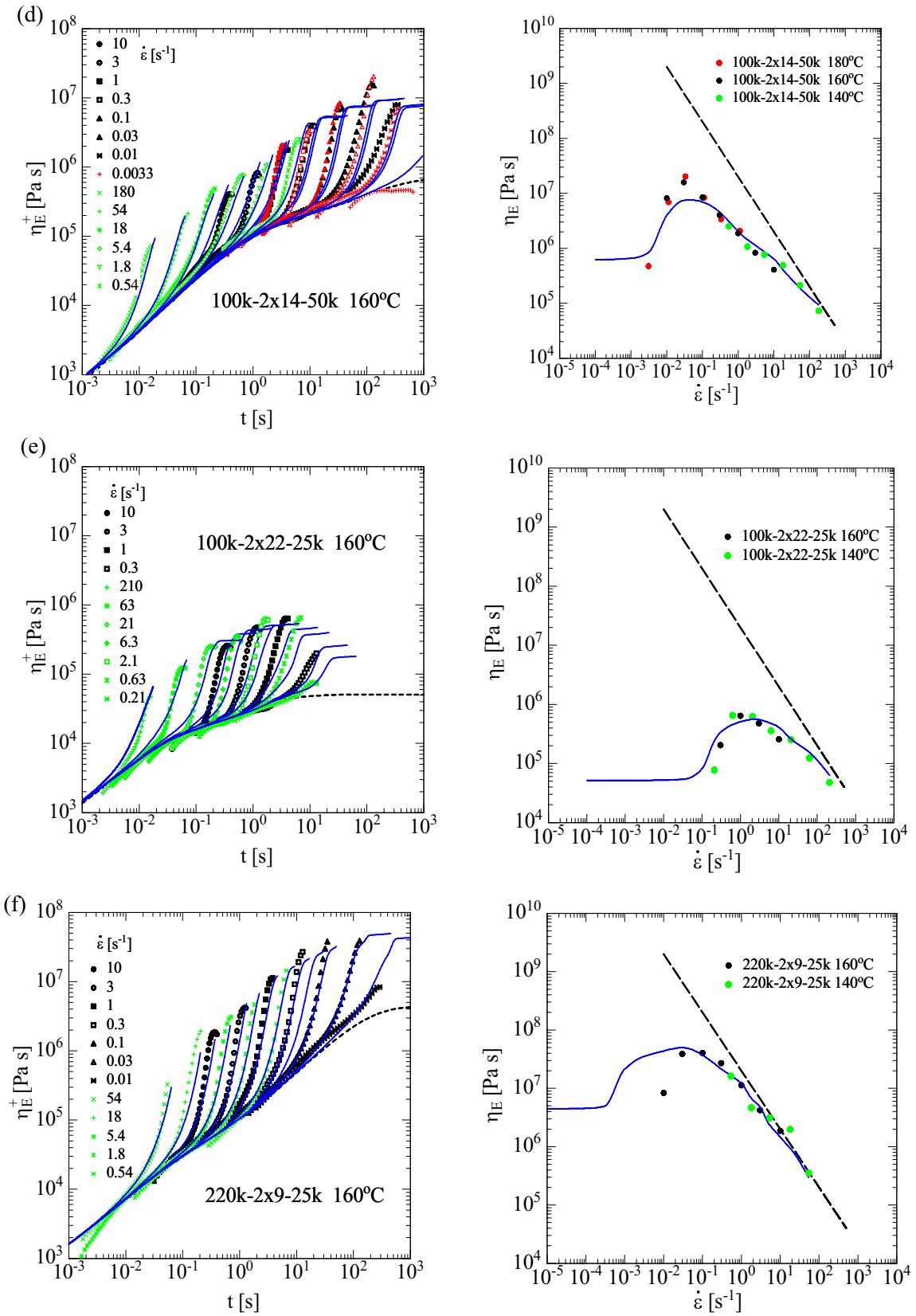

Fig. 6 (continued)

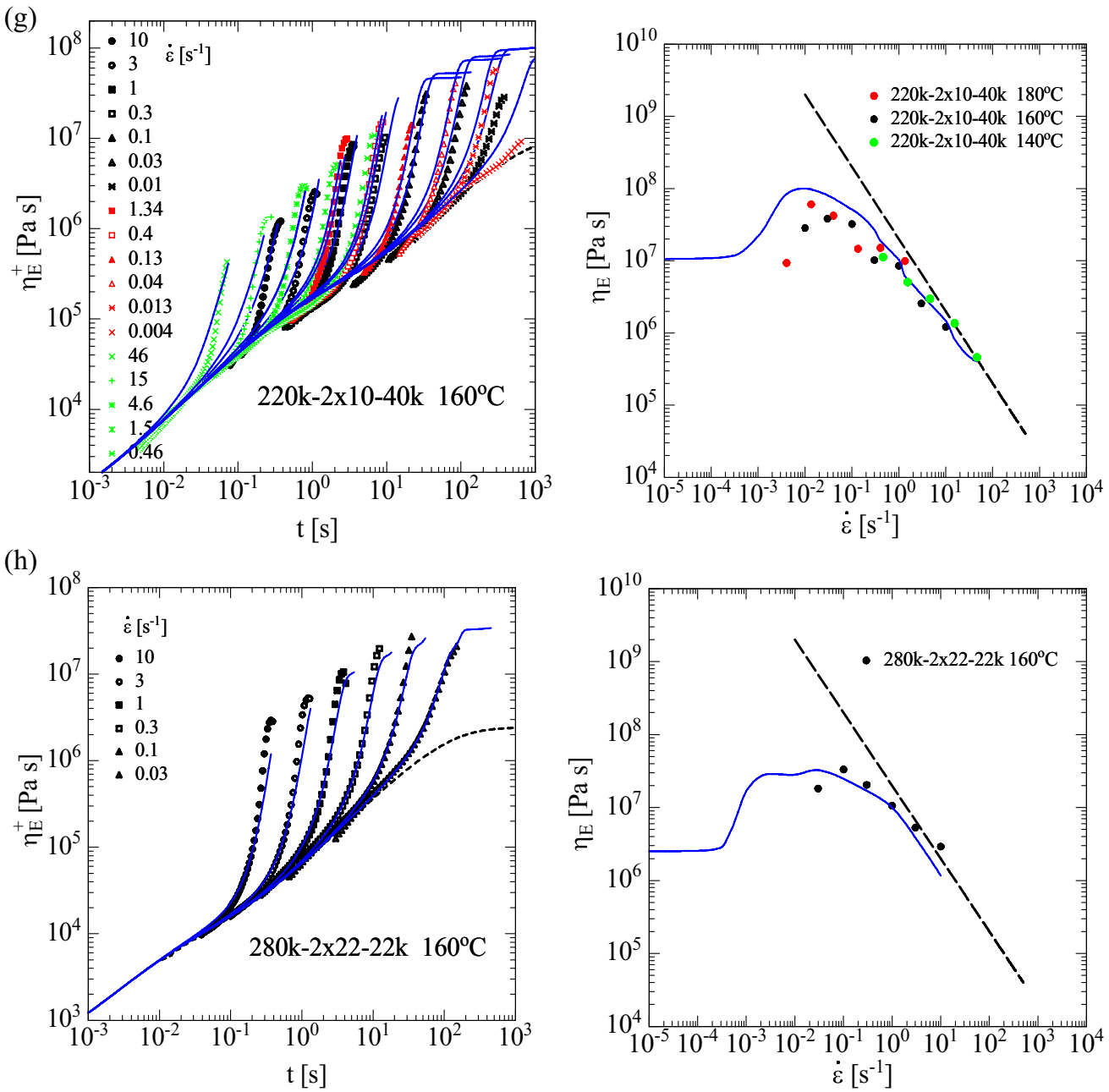

Fig. 6 (continued)

Elongational viscosity and brittle fracture of Pom-Poms

Figure 6 compares the experimental data (symbols) of the elongational stress growth coefficient $\eta_E^+(t)$ and the elongational viscosity $\eta_E(\dot{\varepsilon})$ of the ten Pom-Poms investigated to predictions (lines) of the HMMSF model. The elongational viscosity $\eta_E(\dot{\varepsilon})$ represents the maximal viscosity reached in the experiments (symbols) and predicted by the HMMSF model (lines). Elongational stress growth coefficient data measured at $T = 140$ °C (green symbols) and 180 °C (red symbols) were time-temperature shifted to the reference temperature T_r of 160 °C (black symbols). The shift factors are nearly the same for all Pom-Poms and are displayed in Fig. SI.11. All Pom-Poms show strong strain hardening, i.e., the maximal elongational viscosities η_E are much larger than the linear-viscoelastic start-up viscosity η_E^0 at the corresponding Hencky strain, and the strain hardening factor defined by η_E/η_E^0 reaches values of 2 orders of magnitude with the highest values found for the longest backbones.

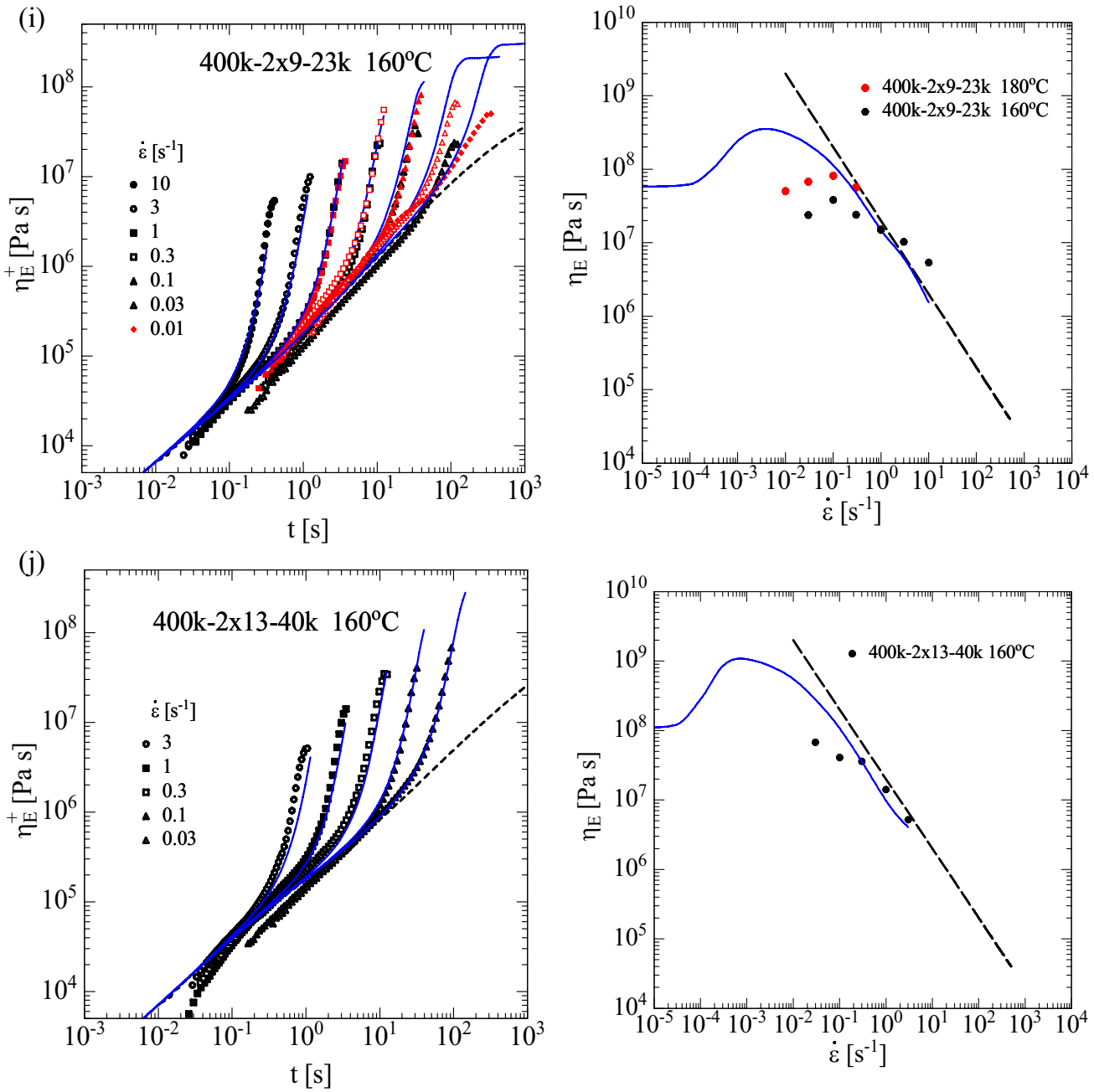

Fig. 6 (continued)

Within experimental accuracy, the elongational stress growth coefficient of the Pom-Pom model systems is well described by the HMMSF model, based exclusively on the linear-viscoelastic relaxation spectra as input and without the use of any further model parameter.

For several Pom-Pom systems, some deviation between experimental data and model is seen at very low strain rates, where the tensile stress is small and approaches the resolution of the force transducer and the accuracy of the measurements might suffer from possible sacking of the samples. The HMMSF model predicts a steady-state elongational viscosity at low strain rates, which is not always reached by the experimental data due to the limitation of the maximum Hencky strain of $\varepsilon = 4$. At larger strain rates, the Pom-Pom samples fracture due to their high elasticity, which is well described by the fracture criterion of Eq. (8). The data reveal an effective limiting fracture stress of $\sigma_E^{Fracture} = 2.0 \times 10^7$ Pa (broken line in the $\eta_E(\dot{\varepsilon})$ plots), which is in good agreement with the experimental data and corresponds within a factor of order 1 with the maximal fracture stress predicted by the HMMSF model according to Eq. (9).

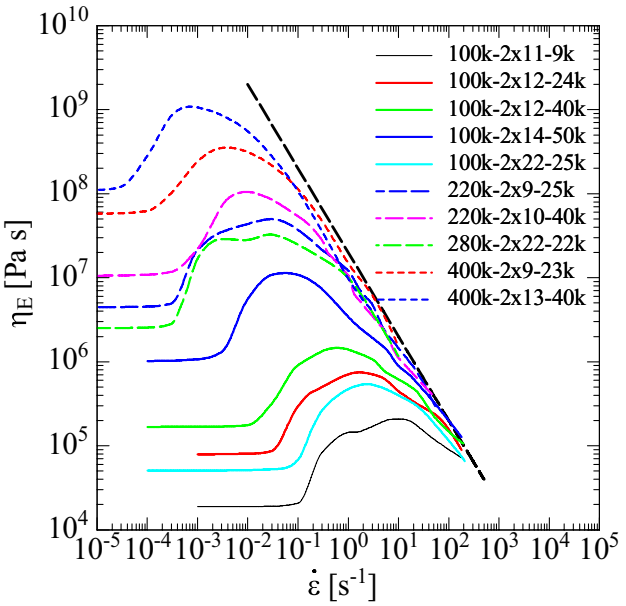

Fig. 7 Maximal elongational viscosity $\eta_E(\dot{\epsilon})$ as predicted by the HMMSF model. Broken straight black line with a slope of − 1 line represents the limiting fracture stress of $\sigma_E^{Fracture} = 2.010^7$Pa

We recall that the specific type of the molecular topology has a paramount impact on linear viscoelasticity and that the SAOS mastercurve, which is the input of the HMMSF model, reflects the full information on relaxation times and relaxation strengths of backbone and arms including their interactions. Up to now, the HMMSF model has been applied mainly to polydisperse linear polymers or polymers with a randomly branched topology, and the dilution effect due to the unknown concentration of oligomers, chain ends, and short side chains could be collapsed in elongational flow into a single parameter, the dilution modulus G_D. For the Pom-Pom melts with many side arms and with low dispersity considered here, the equivalence of G_D and the plateau modulus G_N^0 emphasizes the importance of dynamic dilution for nonlinear viscoelasticity and at the same time points to the similarity of the underlying mechanisms determining the elongational strain hardening of randomly branched systems. Consequently, if the SAOS mastercurve of a branched polymer system is known, strain hardening can be predicted within a single parameter, the dilution modulus G_D, which on the other hand highlights the importance of predicting the SAOS mastercurve directly from polymer topology.

Figure 7 presents a comparison of the HMMSF model predictions of the maximal elongational viscosity $\eta_E(\dot{\epsilon})$ for all ten Pom-Poms. The elongational viscosity $\eta_E(\dot{\epsilon})$ approaches the limiting fracture stress of $\sigma_E^{Fracture} = 2.0 \times 10^7$Pa at higher strain rates and increases both with the arm length and the backbone length of the Pom-Poms.

The effect of the increase of arm length at constant backbone molecular weight $M_{w,b}$ of 100 kg/mol and at approximately constant number q_a of arms is shown in Fig. 8. Increasing the molecular weight $M_{w,a}$ of the arms

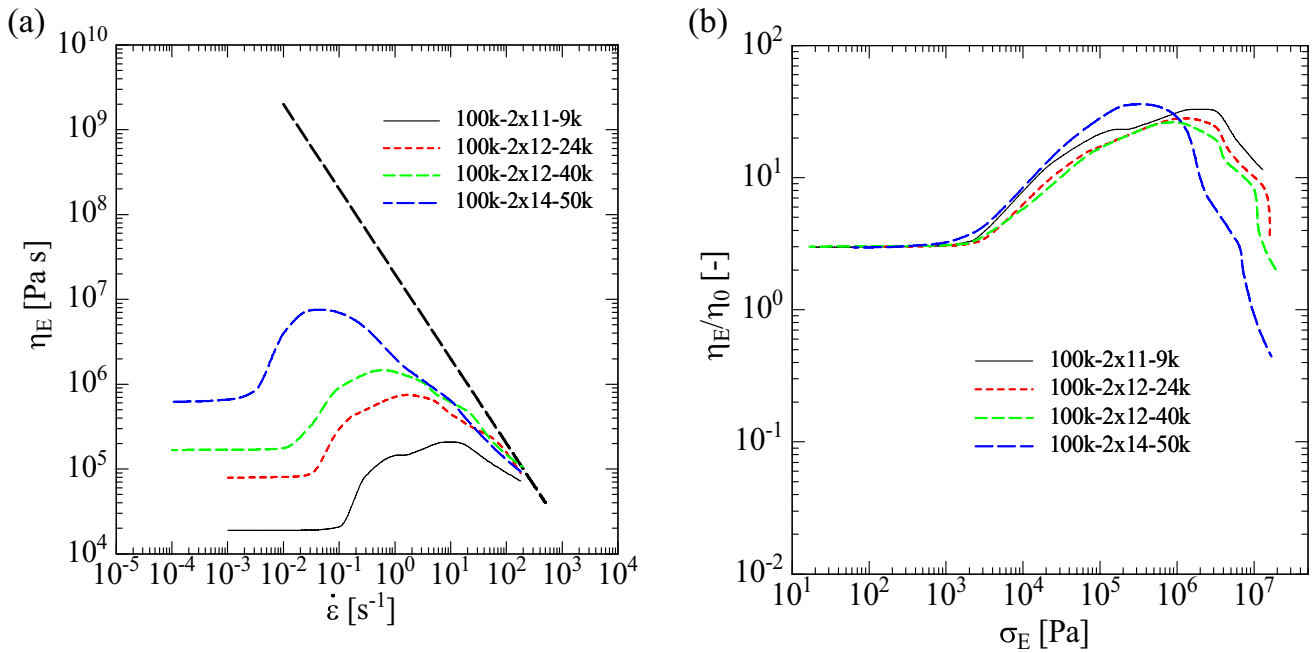

Fig. 8 Effect of arm length at constant backbone molecular weight $M_{w,b}$ of 100 kg/mol and at approximately constant number of arms q_a on **a** maximal elongational viscosity η_E as a function of strain rate $\dot{\epsilon}$ and on **b** normalized maximal elongational viscosity η_E/η_0 as a function of maximal elongational stress σ_E

increases the zero-elongational viscosity and shifts $\eta_E(\dot{\varepsilon})$ in Fig. 8a approximately under − 45 degrees upwards. The normalized elongational viscosity η_E/η_0 is plotted as a function of the tensile stress σ_E in Fig. 8b. This temperature invariant representation reveals that while the maximum of η_E/η_0 is largely independent of the molecular weight $M_{w,a}$ of the arms, there is a tendency that the maximum occurs at lower values of σ_E with increasing $M_{w,a}$. If the potential for strain hardening of a polymer system is assessed by the maximum of the ratio η_E/η_0, all 4 Pom-Poms show the same strain hardening with a maximal value of $\eta_E/\eta_0 \approx 30$. Changing the number q_a of arms from 2×12 to 2×22 at nearly constant arm molecular weight $M_{w,a}$ of 24 or 25 kg/mol does not significantly affect the shape of $\eta_E(\dot{\varepsilon})$, but reduces the zero-elongational viscosity due to the dilution effect of the arms as shown in Fig. 9. However, we note that the number of 2×12 arms of Pom-Pom 100 k-$2\times$12-24 k is already large enough to cause dynamic dilution starting from the plateau modulus G_N^0. In contrast, Nielsen et al. (2006a,b) investigated a pom-pom melt with (on average) 2.5 arms per backbone end, which according to our nomenclature has the designation 140 k-$2\times$2.5-28 k. As shown by Wagner et al. (2022), the elongational stress growth coefficient $\eta_E^+(t)$ of this pom-pom melt is consistent with a much smaller dilution modulus of $G_D = 6.0 \cdot 10^4 Pa \approx G_N^0/4$ corresponding to the mass fraction of the backbone of $\varphi_{BB} = 0.5$. It seems that the relative small number of 2.5 arms leads to permanent dilution of the backbone of pom-pom 140 k-$2\times$2.5-28 k

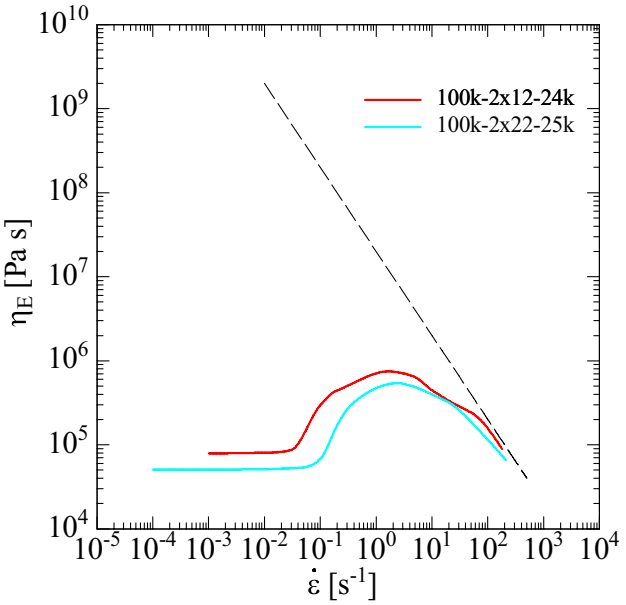

Fig. 9 Effect of number of arms q_a at constant backbone molecular weight $M_{w,b}$ of 100 kg/mol and nearly constant arm molecular weight mass $M_{w,a}$ of 24 or 25 kg/mol on maximal elongational viscosity $\eta_E(\dot{\varepsilon})$

in the experimental window, and dynamic dilution starts only at $G_D < G_N^0$. Consequently, strain hardening and the maximal value of η_E/η_0 for pom-pom 140 k-$2\times$2.5-28 k is much smaller with $\eta_E/\eta_0 \approx 8$ than for Pom-Pom 100 k-$2\times$12-24 k or any other of the Pom-Poms investigated here. We may conclude that a minimum threshold number of arms may be required to guarantee the full potential of dynamic dilution, and further investigation is under way to determine this threshold condition.

Increasing the backbone molecular weight $M_{w,b}$ at approximately constant number of arms (q_a of 2×9 to 2×13) with arm molecular weight $M_{w,a}$ of 23 to 25 kg/mol (Fig. 10a) and $M_{w,a}$ of 40 kg/mol (Fig. 10c), respectively, increases the zero-elongational viscosity and shifts $\eta_E(\dot{\varepsilon})$ again under − 45 degrees upwards. Similar shapes of the normalized elongational viscosity curves are obtained if the normalized elongational viscosity η_E/η_0 is plotted as a function of the tensile stress σ_E (Fig. 10b and d). This indicates a similar strain hardening potential independent of the backbone molecular weight again with a maximal value of $\eta_E/\eta_0 \approx 30$. Comparing Fig. 10b and d, we note again a tendency that the maximum occurs at a lower value of σ_E with increasing $M_{w,a}$.

Conclusions

We have analyzed the rheological data of ten low-dispersive Pom-Pom model systems with systematically varied molecular properties. The molecular weights of the backbone, $M_{w,b}$, and of the arms, $M_{w,a}$, cover the range from $M_{w,b} = 100$ to 400 kg/mol and from $M_{w,a} = 9$ to 50 kg/mol, respectively, and the number of arms q_a varies between 9 and 22 arms per backbone end. The main conclusions of this analysis are:

1. The plateau modulus G_N^0 of all ten Pom-Pom melts is of the order of 2.0×10^5 Pa as expected for polystyrene.
2. Due to the high number of arms, four out of the five Pom-Poms with backbone molecular weight of $M_{W,BB} = 100$ kg/mol have volume fractions of $\phi_{BB} \leq 0.15$ and show only one low-frequency cross-over of G' and G''. After dynamic relaxation by the arms, the backbones are unentangled and relax by constraint Rouse relaxation.
3. Pom-Pom 100 k-$2\times$11-9 k and Pom-Poms with backbone molecular weights of $M_{w,b} = 220$ to 400 kg/mol have higher volume fractions $\phi_{BB} \leq 0.22$ of the backbone and show two distinct minima of $\tan\delta(G')$, representing the plateau modulus G_N^0 of the Pom-Pom molecule and the plateau modulus $G_{N,s}^0$ of the dynamically diluted backbone chains.
4. The modulus $G_{N,s}^0$ of the dynamically diluted backbone chains is related to the plateau G_N^0 by $G_{N,s}^0 \cong G_N^0 \varphi_{BB}^2$, if

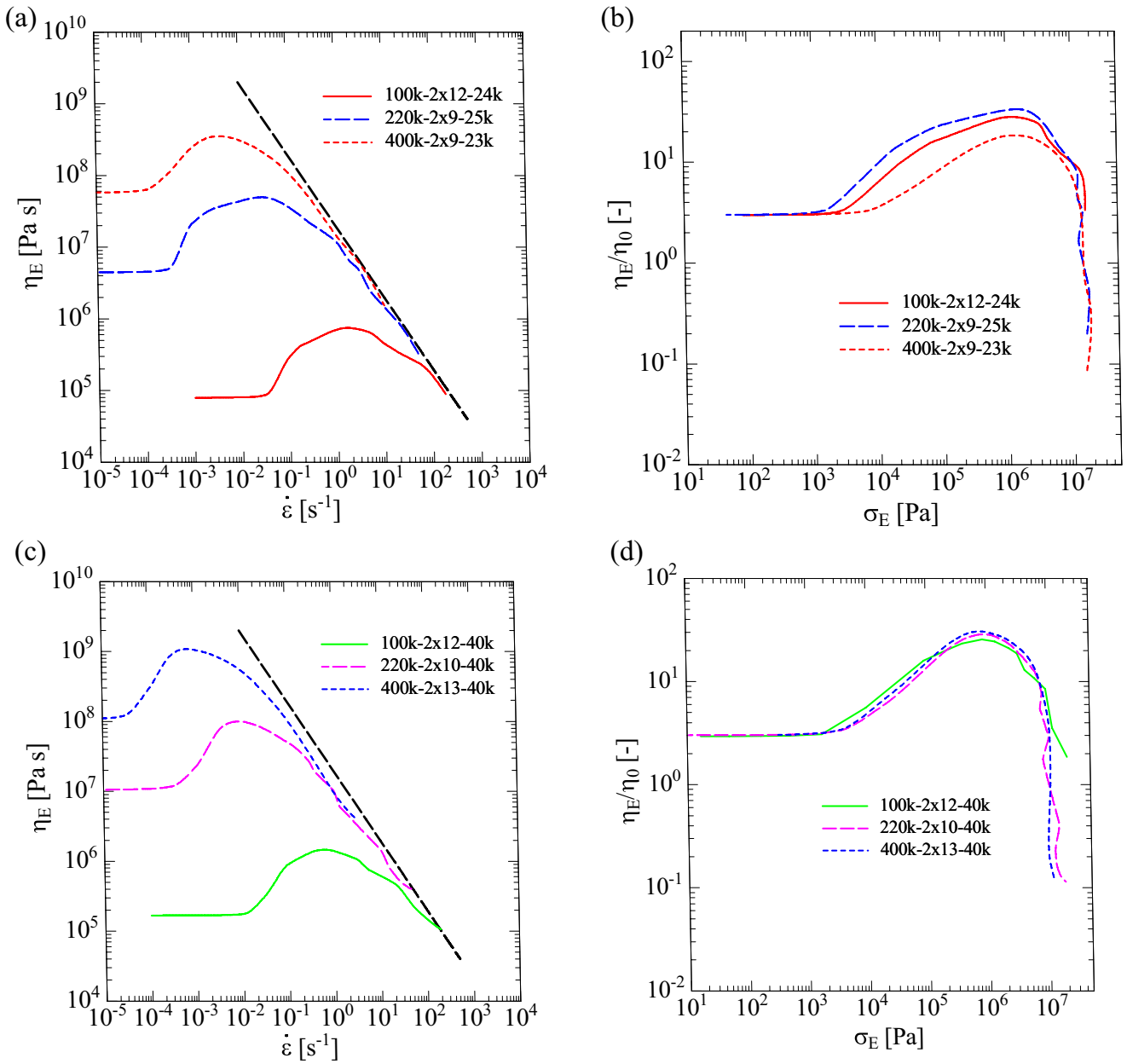

Fig. 10 Effect of backbone length on maximal elongational viscosity η_E as a function of strain rate $\dot{\epsilon}$ and on normalized maximal elongational viscosity η_E/η_0 as a function of maximal elongational stress σ_E at approximately constant number of arms (q_a of 2×9 to 2×13) and arm molecular weight $M_{w,a}$ of 23 to 25 kg/mol (**a** and **b**) and $M_{w,a}$ of 40 kg/mol (**c** and **d**), respectively

the backbone chains remain entangled after relaxation of the arms.

5. All ten Pom-Pom melts show a strong increase of the elongational stress growth coefficient $\eta_E(t)$, which exceeds the linear-viscoelastic start-up viscosity $\eta_E^0(t)$ greatly by up to 2 orders of magnitude. This is usually taken as the signature of "strain hardening" in elongational flow.
6. The strain-hardening effect does not depend on whether the arms are entangled or not or whether after dynamic dilution by the arms, the backbones remain entangled or not.
7. At larger strain rates and strains in elongational flow, all Pom-Pom melts investigated are subject to sample failure by brittle fracture.
8. Within experimental accuracy, the elongational stress growth coefficient is well described by the HMMSF model, based exclusively on the linear-viscoelastic relaxation spectrum and the plateau modulus G_N^0 as input and without the use of any further model param-

eter. Permanent dilution caused by possibly remaining traces of solvent is already reflected by the plateau modulus. For the 10 Pom-Poms with many side arms considered here, dynamic dilution starts at the plateau modulus G_N^0 by hierarchical relaxation of the arms followed by relaxation of the backbone chains. This is independent of whether arms are entangled or not entangled and whether the backbone chains remain self-entangled or are not self-entangled after dynamic dilution by the arms. However, we note that for Pom-Poms with a smaller number of arms, dynamic dilution may start at a dilution modulus $G_D < G_N^0$ resulting in smaller strain hardening. Apparently, a minimum threshold number of arms seem to be required to guarantee the full potential of dynamic dilution, and further investigation is needed to determine this threshold.

9. Within experimental accuracy, the entropic fracture criterion describes the occurrence of brittle fracture quantitatively. For all ten Pom-Pom systems and the elongation rate range investigated, an effective limiting fracture stress of $\sigma_E^{Fracture} = 2.0 \times 10^7$Pa is found, which agrees within a factor of order 1 with the maximal fractures stress of 160 G_N^0 expected at very high strain rates according to Eq. (10).
10. Increasing the molecular weight of the arms $M_{w,a}$ at constant number of arms q_a and constant molecular weight of the backbone $M_{w,b}$ increases the zero-elongational viscosity.
11. Increasing the number of arms q_a at constant molecular weight of the arms $M_{w,a}$ and at constant molecular weight of the backbone $M_{w,b}$ reduces the zero-elongational viscosity.
12. Increasing the backbone molecular weight $M_{w,b}$ at constant arm number q_a and arm molecular weight $M_{w,a}$ increases the zero-elongational viscosity.
13. The maximum of the normalized elongational viscosity η_E/η_0 is largely independent of the arm molecular weight $M_{w,a}$ and the backbone molecular weight $M_{w,b}$. There is a tendency that the maximum of η_E/η_0 occurs at a lower value of σ_E with increasing $M_{w,a}$.
14. If the potential for strain hardening of a polymer system is assessed by the maximum ratio η_E/η_0, all Pom-Poms investigated show a similar amount of strain hardening with a maximal value of $\eta_E/\eta_0 \approx 30$.

Supplementary information The online version contains supplementary material available at https://doi.org/10.1007/s00397-023-01393-0.

Acknowledgements We thank Michael Pollard for English proof reading as a native speaker.

Funding Open Access funding enabled and organized by Projekt DEAL.

Data Availability Additionally, most raw data are provided in the SI.

Declarations

Conflict of interest The authors declare no competing interests.

References

Abbasi M, Faust L, Riazi K, Wilhelm M (2017) Linear and extensional rheology of model branched polystyrenes: from loosely grafted combs to bottlebrushes. Macromolecules 50:5964–5977. https://doi.org/10.1021/acs.macromol.7b01034

Abbasi M, Faust L, Wilhelm M (2019) Comb and bottlebrush polymers with superior rheological and mechanical properties. Adv Mater 31:e1806484. https://doi.org/10.1002/adma.201806484

Doi M, Edwards SF (1978) Dynamics of concentrated polymer systems. Part 3.—The constitutive equation. J Chem Soc Faraday Trans 2(74):1818–1832. https://doi.org/10.1039/F29787401818

Doi M, Edwards SF (1979) Dynamics of concentrated polymer systems. Part 4.—Rheological properties. J Chem Soc Faraday Trans 2(75):38–54. https://doi.org/10.1039/F29797500038

Faust L, Ropert MC, Esfahani MK, Abbasi M, Hirschberg V, Wilhelm M (2022) Comb and branch-on-branch model polystyrenes with exceptionally high strain hardening factor SHF > 1000 and their impact on physical foaming. Macromol Chem Phys. https://doi.org/10.1002/macp.202200214

Frischknecht AL, Milner ST, Pryke A, Young RN, Hawkins R, McLeish TCB (2002) Rheology of three-arm asymmetric star polymer melts. Macromolecules 35:4801–4820. https://doi.org/10.1021/ma0101411

Graessley WW, Roovers J (1979) Melt rheology of four-arm and six-arm star polystyrenes. Macromolecules 12:959–965. https://doi.org/10.1021/ma60071a035

Houli S, Iatrou H, Hadjichristidis N, Vlassopoulos D (2002) Synthesis and viscoelastic properties of model dumbbell copolymers consisting of a polystyrene connector and two 32-arm star polybutadienes. Macromolecules 35:6592–6597. https://doi.org/10.1021/ma0204709

Huang Q (2022) When polymer chains are highly aligned: a perspective on extensional rheology. Macromolecules 55(3):715–727. https://doi.org/10.1021/acs.macromol.1c02262

Huang Q, Hassager O (2017) Polymer liquids fracture like solids. Soft Matter 13:3470–3474. https://doi.org/10.1039/C7SM00126F

Huang Q, Alvarez NJ, Shabbir A, Hassager O (2016) Multiple cracks propagate simultaneously in polymer liquids in tension. Phys Rev Lett 117:87801. https://doi.org/10.1103/PhysRevLett.117.087801

Ianniello V, Costanzo S (2022) Linear and nonlinear shear rheology of nearly unentangled H-polymer melts and solutions. Rheol Acta 61:667–679. https://doi.org/10.1007/s00397-022-01349-w

Ianniruberto G, Marrucci G, Masubuchi Y (2020) Melts of linear polymers in fast flows. Macromolecules 53:5023–5033. https://doi.org/10.1021/acs.macromol.0c00693

Kapnistos M, Vlassopoulos D, Roovers J, Leal LG (2005) Linear rheology of architecturally complex macromolecules: comb polymers with linear backbones. Macromolecules 38:7852–7862. https://doi.org/10.1021/ma050644x

Kempf M, Ahirwal D, Cziep M, Wilhelm M (2013) Synthesis and linear and nonlinear melt rheology of well-defined comb architectures of PS and PpMS with a low and controlled degree of long-chain branching. Macromolecules 46:4978–4994. https://doi.org/10.1021/ma302033g

Larson RG (1999) The structure and rheology of complex fluids. Oxford University Press, New York [etc.]

Lentzakis H, Vlassopoulos D, Read DJ, Lee H, Chang T, Driva P, Hadjichristidis N (2013) Uniaxial extensional rheology of well-characterized comb polymers. J Rheol 57:605. https://doi.org/10.1122/1.4789443

Lentzakis H, Costanzo S, Vlassopoulos D, Colby RH, Read DJ, Lee H, Chang T, van Ruymbeke E (2019) Constraint release mechanisms for h-polymers moving in linear matrices of varying molar masses. Macromolecules 52:3010–3028. https://doi.org/10.1021/acs.macromol.9b00251

Matsumiya Y, Watanabe H (2021) Non-universal features in uniaxially extensional rheology of linear polymer melts and concentrated solutions: a review. Prog Polym Sci 112:101325. https://doi.org/10.1016/j.progpolymsci.2020.101325

Matsumiya Y, Watanabe H, Masubuchi Y, Huang Q, Hassager O (2018) Nonlinear elongational rheology of unentangled polystyrene and poly(p - tert- butylstyrene) melts. Macromolecules 51:9710–9729. https://doi.org/10.1021/acs.macromol.8b01954

McLeish TCB, Larson RG (1998) Molecular constitutive equations for a class of branched polymers: the pom-pom polymer. J Rheol 42:81–110. https://doi.org/10.1122/1.550933

McLeish TCB, Allgaier J, Bick DK, Bishko G, Biswas P, Blackwell R, Blottière B, Clarke N, Gibbs B, Groves DJ, Hakiki A, Heenan RK, Johnson JM, Kant R, Read DJ, Young RN (1999) Dynamics of entangled H-polymers: theory, rheology, and neutron-scattering. Macromolecules 32:6734–6758. https://doi.org/10.1021/ma990323j

Moingeon F, Wu YR, Cadena-Sánchez LE, Gauthier M (2012) Synthesis of arborescent styrene homopolymers and copolymers from epoxidized substrates. J Polym Sci A Polym Chem 50:1819–1826. https://doi.org/10.1002/pola.25951

Narimissa E, Wagner MH (2016a) A hierarchical multimode molecular stress function model for linear polymer melts in extensional flows. J Rheol 60:625–636. https://doi.org/10.1122/1.4953442

Narimissa E, Wagner MH (2016b) A hierarchical multi-mode MSF model for long-chain branched polymer melts part III: shear flows. Rheol Acta 55:633–639. https://doi.org/10.1007/s00397-016-0939-2

Narimissa E, Wagner MH (2016c) From linear viscoelasticity to elongational flow of polydisperse linear and branched polymer melts: the hierarchical multi-mode molecular stress function model. Polymer 104:204–214. https://doi.org/10.1016/j.polymer.2016.06.005

Narimissa E, Wagner MH (2019a) Review of the hierarchical multi-mode molecular stress function model for broadly distributed linear and LCB polymer melts. Polym Eng Sci 59:573–583. https://doi.org/10.1002/pen.24972

Narimissa E, Wagner MH (2019b) Review on tube model based constitutive equations for polydisperse linear and long-chain branched polymer melts. J Rheol 63:361–375. https://doi.org/10.1122/1.5064642

Narimissa E, Rolón-Garrido VH, Wagner MH (2015) A hierarchical multi-mode MSF model for long-chain branched polymer melts part I: elongational flow. Rheol Acta 54:779–791. https://doi.org/10.1007/s00397-015-0879-2

Narimissa E, Rolón-Garrido VH, Wagner MH (2016) A hierarchical multi-mode MSF model for long-chain branched polymer melts part II: multiaxial extensional flows. Rheol Acta 55:327–333. https://doi.org/10.1007/s00397-016-0922-y

Nielsen JK, Rasmussen HK, Hassager O, McKinley G (2006a) Elongational viscosity of monodisperse and bidisperse polystyrene melts. J Rheol 50:453. https://doi.org/10.1122/1.2206711

Nielsen JK, Rasmussen HK, Denberg M, Almdal K, Hassager O (2006b) Nonlinear branch-point dynamics of multiarm polystyrene. Macromolecules 39:8844–8853. https://doi.org/10.1021/ma061476r

Poh L, Narimissa E, Wagner MH, Winter HH (2022) Interactive shear and extensional rheology—25 years of IRIS software. Rheol Acta 61:259–269. https://doi.org/10.1007/s00397-022-01331-6

Roovers J, Graessley WW (1981) Melt rheology of some model comb polystyrenes. Macromolecules 14:766–773. https://doi.org/10.1021/ma50004a057

Röpert M-C, Schußmann MG, Esfahani MK, Wilhelm M, Hirschberg V (2022a) Effect of side chain length in polystyrene POM–POMs on melt rheology and solid mechanical fatigue. Macromolecules. https://doi.org/10.1021/acs.macromol.2c00199

Röpert et al. (2022b) Threading Polystyrene Stars: Impact of Star to POM-POM and Barbwire Topology on Melt Rheological and Foaming Properties. MC Röpert, A Goecke, M Wilhelm, V Hirschberg Macromolecular Chemistry and Physics, 2200288. https://doi.org/10.1002/macp.202200288

Stadler FJ, Kaschta J, Münstedt H, Becker F, Buback M (2009) Influence of molar mass distribution and long-chain branching on strain hardening of low density polyethylene. Rheol Acta 48:479–490. https://doi.org/10.1007/s00397-008-0334-8

van Ruymbeke E, Kapnistos M, Vlassopoulos D, Huang T, Knauss DM (2007) Linear melt rheology of pom-pom polystyrenes with unentangled branches. Macromolecules 40:1713–1719. https://doi.org/10.1021/ma062487n

van Ruymbeke E, Muliawan EB, Hatzikiriakos SG, Watanabe T, Hirao A, Vlassopoulos D (2010) Viscoelasticity and extensional rheology of model Cayley-tree polymers of different generations. J Rheol 54:643–662. https://doi.org/10.1122/1.3368724

Wagner MH, Rubio P, Bastian H (2001) The molecular stress function model for polydisperse polymer melts with dissipative convective constraint release. J Rheol 45:1387–1412. https://doi.org/10.1122/1.1413503

Wagner MH, Kheirandish S, Yamaguchi M (2004) Quantitative analysis of melt elongational behavior of LLDPE/LDPE blends. Rheol Acta 44:198–218. https://doi.org/10.1007/s00397-004-0400-9

Wagner MH, Narimissa E, Huang Q (2018) On the origin of brittle fracture of entangled polymer solutions and melts. J Rheol 62:221–233. https://doi.org/10.1122/1.4995497

Wagner MH, Narimissa E, Poh L, Huang Q (2022) Modelling elongational viscosity overshoot and brittle fracture of low-density polyethylene melts. Rheol Acta 61:281–298. https://doi.org/10.1007/s00397-022-01328-1

Winter HH, Mours M (2006) The cyber infrastructure initiative for rheology. Rheol Acta 45:331–338. https://doi.org/10.1007/s00397-005-0041-7

Yuan Z, Gauthier M (2005) Synthesis of arborescent isoprene homopolymers. Macromolecules 38:4124–4132. https://doi.org/10.1021/ma0479565